Author Manuscript

Author Manuscript

Author Manuscript

Author Manuscript

HHS Public Access

Author manuscript

Biochemistry. Author manuscript; available in PMC 2020 February 01.

Published in final edited form as:

Biochemistry. 2016 January 12; 55(1): 199–209. doi:10.1021/acs.biochem.5b01099.

The Anchored Flexibility Model in LC8 Motif Recognition: Insights from the Chica Complex

Sarah Clark[†], **Afua Nyarko**[†], **Frank Löhr**[‡], **P. Andrew Karplus**[†], **Elisar Barbar**[*,†]

[†]Department of Biochemistry and Biophysics, Oregon State University, Corvallis, Oregon 97331, United States

[‡]Institute of Biophysical Chemistry, Goethe-University, D-60438 Frankfurt, Germany

Abstract

LC8 is a dimeric hub protein involved in a large number of interactions central to cell function. It binds short linear motifs—usually containing a Thr-Gln-Thr (TQT) triplet—in intrinsically disordered regions of its binding partners, some of which have several LC8 recognition motifs in tandem. Hallmarks of the 7–10 amino acid motif are a high variability of LC8 binding affinity and extensive sequence permutation outside the TQT triplet. To elucidate the molecular basis of motif recognition, we use a 69-residue segment of the human Chica spindle adaptor protein that contains four putative TQT recognition motifs in tandem. NMR-derived secondary chemical shifts and relaxation properties show that the Chica LC8 binding domain is essentially disordered with a dynamically restricted segment in one linker between motifs. Calorimetry of LC8 binding to synthetic motif-mimicking peptides shows that the first motif dominates LC8 recruitment. Crystal structures of the complexes of LC8 bound to each of two motif peptides show highly ordered and invariant TQT-LC8 interactions and more flexible and conformationally variable non-TQT-LC8 interactions. These data highlight rigidity in both LC8 residues that bind TQT and in the TQT portion of the motif as an important new characteristic of LC8 recognition. On the basis of these data and others in the literature, we propose that LC8 recognition is based on rigidly fixed interactions between LC8 and TQT residues that act as an anchor, coupled with inherently flexible interactions between LC8 and non-TQT residues. The “anchored flexibility” model explains the requirement for the TQT triplet and the ability of LC8 to accommodate a large variety of motif sequences and affinities.

Graphical Abstract

[*]**Corresponding Author:** Tel: (541) 737-4143. Fax: (541) 737-0481. barbare@science.oregonstate.edu.

The authors declare no competing financial interest.

Author Manuscript Author Manuscript Author Manuscript Author Manuscript

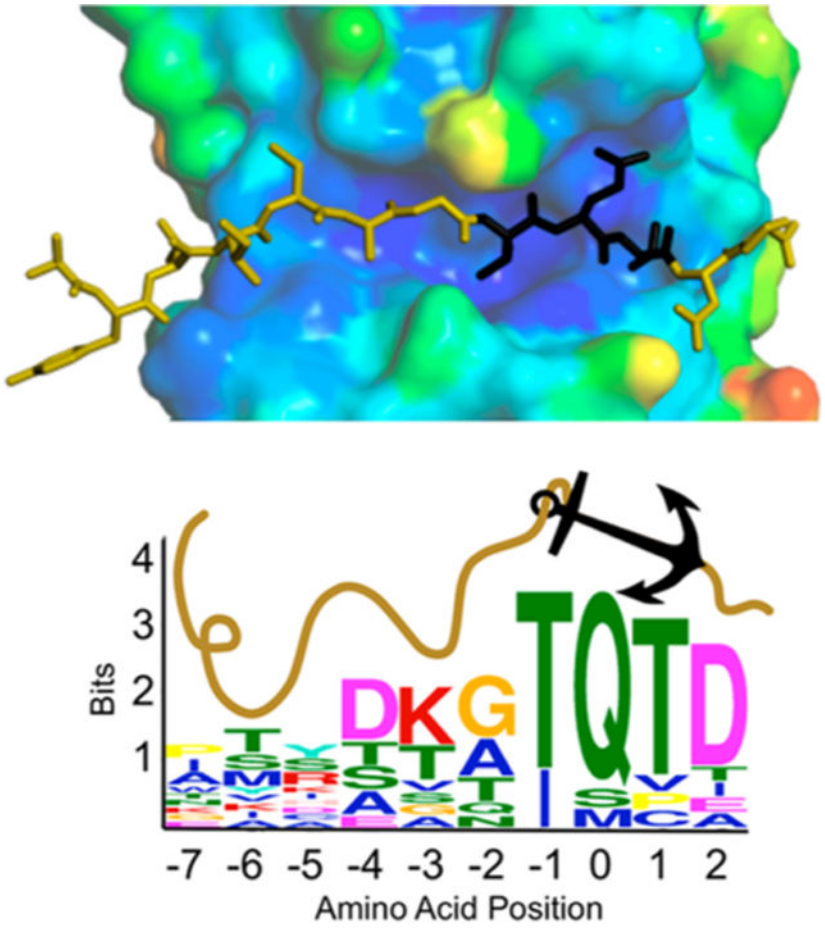

LC8, also known as DLC1 or DYNLL, is a highly conserved, essential protein that interacts with numerous protein partners involved in widely diverse functions. Originally identified as a subunit of the motor complex dynein,[1] LC8 was later shown to be a component of many large multiprotein complexes[2–4] involved in broadly varying processes ranging from tumor suppression to viral replication and DNA damage repair.[5–9] LC8, a homodimer at physiological conditions,[10] invariably binds pairs of the same partner, always a disordered protein or a disordered region of a partially folded protein.[2,11] Crystal structures show that all recognition motifs presented by LC8 partners bind in the same manner to two symmetrical grooves on the LC8 dimer despite their highly variable sequences. The ~10-amino acid recognition motifs are incorporated as antiparallel β-strands.[12–19] In its partner-bound form (Figure 1a), the LC8 dimer is a 12-stranded β-sandwich where each monomer contributes five β-strands (β1–β5, blue), and the recognition motif is the sixth (orange). The antiparallel β-sheet is flanked on each side by pairs of helices (blue).

The 10-amino-acid motif recognized by LC8 includes the signature sequence Thr-Gln-Thr (TQT) at the C-terminus. In a motif logo generated from recognition sequences of 11 crystal structures of LC8/peptide complexes (Figure 1b), residues are numbered from the conserved glutamine at position zero and adjacent residues −1 and 1.[12] While the TQ_0T is an almost universal feature of known motif sequences, other positions show notable conservation, such

Author Manuscript Author Manuscript Author Manuscript Author Manuscript

as aspartate at position 2 and to a smaller extent, residues at −2, −3, and −4. A few partners have different triplet sequences, such as GTQ_0CD in Ana2 and ATS_0PI in Pak1,[14,19] and Q_0 replacement by methionine in myosin 5A[20] or asparagine in Kibra.[21] The variability in motif sequence outside TQ_0T is accompanied by a similarly wide range of binding affinities, from 160 nM to 42 μM.[16,19] In summary, while the TQT triplet is very highly conserved, a diverse array of peptide sequences outside positions TQ_0T are accommodated in the binding groove.

Chica, a protein with multiple LC8 recognition motifs, is a 64-kDa mitotic spindle-associated protein that binds LC8 to form a complex that promotes asymmetrical cortical localization of dynein and correct spindle orientation. Experiments that perturb LC8-Chica association, including LC8 siRNA knockdown or specific mutations of the TQT residues, demonstrate that Chica interaction with LC8 is necessary to target dynein to the cell cortex and to orient mitotic spindles for the proper onset of mitosis.[22] Other proteins in this intriguing group of LC8 partners with multiple recognition motifs include nucleoporin Nup159, with six TQT motifs in tandem of which five bind LC8,[23] and the transcription factor ASCIZ with 17 motifs of which 11 bind LC8.[24] Chica has four conserved TQT motifs (QT1–4) within the intrinsically disordered segment of its C-terminal half (Figure 2). Mutation of the TQT sequences within QT1, QT2, and QT4 completely abolish binding to LC8,[22] a strong indication that LC8 does not bind QT3. The one-residue linker separating QT2 and QT3 implies that only one of these can bind LC8.

Here, using nuclear magnetic resonance spectroscopy (NMR), isothermal titration calorimetry (ITC), and X-ray crystallography, we have determined structural and dynamic properties of the LC8 binding domain of Chica and the thermodynamic and structural characteristics of its interactions with LC8. These studies were carried out on a 69-amino acid Chica construct containing the four TQT recognition motifs and on short synthetic peptides corresponding to each of the recognition motifs. We show which TQT motif does not bind LC8, and of the three that do bind, which dominates LC8 recruitment by Chica. Our findings with Chica support a model of LC8-motif binding that is anchored by a set of favorable and conserved interactions with the TQT residues, and that is modulated in a difficult-to-predict manner by the variable residues at other motif positions that serve to decrease or enhance the overall affinity.

MATERIALS AND METHODS

Cloning, Protein Expression, and Purification.

A gene encoding mammalian Chica (FAM83D, accession number NP112181) residues 410–478 was synthesized (GenScript, Piscataway, NJ), subcloned into pET15 vector (Novagen) which added a a 17 non-native residue extension containing a hexahistidine tag, and the construct was transformed into *Escherichia coli* BL21-DE3 cell line. *E. coli* strains were grown at 37 °C in LB or in minimal media with ^{12}C or ^{13}C glucose, and $^{15}NH_4Cl$ as the sole carbon and nitrogen sources, respectively. Recombinant protein overexpression was induced with 0.2 mM IPTG and growth continued at 18 °C for 12 h. Cells were harvested and purified under native conditions using Qiagen's Ni-NTA purification protocol (Qiagen). Recombinant proteins were further purified on a SuperdexTM 75 gel filtration column (GE Health). The purity of the recombinant His-tagged protein, as assessed by SDS

Author Manuscript Author Manuscript Author Manuscript Author Manuscript

polyacrylamide gels, was >95%. The His tag was not removed to improve solubility, and we anticipate it has a minimal effect on structure and interactions, as interactions identified with this domain (see below) are similar to the interactions identified in the full-length protein.[22] The pure protein was stored at 4 °C and used within 2 weeks. LC8 was overexpressed and purified as previously described.[10]

Peptide Design and Synthesis.

Peptides corresponding to the four putative recognition sequences, SYRKAIDAATQTEE (QT1p), SYSVSEVGTQTSI (QT2p), SYTTACAGTQTAV (QT3p), and SYWSRSTTTQTDM (QT4p) were synthesized (GenScript, Piscataway, NJ). Non-native residues (Table 1, underlined) were added to the N-terminus of each peptide to facilitate solubility and peptide concentration determination by absorbance at 280 nm. In QT1p, the C-terminal Glu replaces a Pro residue in the wild type sequence to increase solubility. This replacement is justified as in the crystal structure the side chain of E425 in QT1p does not form a hydrogen bond with LC8, suggesting minimal contribution to binding affinity from the replacement.

Isothermal Titration Calorimetry.

Binding thermodynamics of the $Chica_{410–478}$/peptide-LC8 interactions were obtained at 25 °C with a VP-ITC microcalorimeter (Microcal). Chica peptides were dissolved in the reaction buffer composed of 50 mM sodium phosphate, 50 mM sodium chloride, 0.5 mM sodium azide, pH 7.5 to final concentrations of 280–300 μM and then added to 30–35 μM of LC8 in the reaction cell. For binding to $Chica_{410–478}$, LC8 at a concentration of 280 μM was titrated into 10 μM $Chica_{410–478}$ in the reaction cell. Peak areas were integrated and fitted to a single-site binding model in Origin 7.0 from which the stoichiometry (N), dissociation constant (K_d), the change in enthalpy (ΔH) and entropy (ΔS) were obtained. Reported data are the average of three independent experiments.

Circular Dichroism.

CD data were collected on a Jasco720 spectropolarimeter. Three scans collected at 1 nm step resolution, and 1.0 nm bandwidth were averaged for the spectrum of $Chica_{410–478}$ at a concentration of 10 μM in buffer composed of 10 mM sodium phosphate, pH 7.3. The temperature of the experiment was maintained at 25 °C by connecting the 1 mm water-jacketed sample cell to a water bath.

NMR Experiments.

NMR measurements were collected at 15 °C, using 150–250 μM isotopically (^{15}N or $^{13}C/^{15}N$) labeled $Chica_{410–478}$ in buffer composed of 10 mM sodium phosphate, 10 mM sodium chloride, 1 mM sodium azide, pH 7.0, with 50 mM arginine/glutamate (to improve solubility[25]), a protease inhibitor mixture (Roche Applied Science), and 2,2-dimethylsilapentane-5-sulfonic acid for ^1H chemical shifts referencing. All experiments were collected on a Bruker Avance 600 spectrometer equipped with a cryoprobe. The CA, CB, N, CO, and HA chemical shifts were assigned from 2D [^{15}N,^1H] BEST-TROSY,[25,26] 3D- BEST-TROSY-HNCACB and HN(CO)-CACB, and 3D-BEST-TROSY-HNCO, and

Author Manuscript Author Manuscript Author Manuscript Author Manuscript

HA(CACON)H. T_1 relaxation measurements experiments were recorded with relaxation delay times ranging from 10 to 900 ms, and the T_2 relaxation data were acquired using relaxation delays ranging from 22.72 to 318.08 ms. Curve fitting was done with the rate analysis interface of NMRview.[27] Steady-state $^{1}H–^{15}N$ hetero-nuclear NOE acquired with TROSY detection were based on described methods using 6 s total saturation time.[28,29] Unless otherwise stated, all spectra were processed with Topspin (Bruker Biosciences) and analyzed with Sparky.[30] NMR titration experiments with LC8 were attempted, but data collection was hampered by the propensity of $Chica_{410–478}$ to aggregate during the titration.

Protein Crystallization and Structure Determination.

Crystals grew within 2 weeks at room temperature using the hanging-drop, vapor diffusion method. For the QT1p complex, hexagonal rods were grown by mixing a solution of 0.8 mM LC8 and 2 mM QT1p in 20 mM Tris (pH 8.0) in a 1:1 (v/v) drop with a reservoir solution of 0.1 M calcium acetate, 0.1 M sodium cacodylate, 15% polyethylene glycol 8000 (pH 5.5). For the QT4p complex, rounded barrel-shaped crystals were grown using the same LC8 stock but a large excess of QT4p and a reservoir solution of 0.2 M lithium sulfate, 0.1 M Bis-Tris, 25% polyethylene glycol 3350 (pH 5.5). Crystals were transferred to a cryoprotectant consisting of reservoir solution plus 20% (v/v) glycerol, and then flash-frozen on nylon loops in liquid nitrogen.

Diffraction data were collected on beamline 5.0.2 at the Advanced Light Source, Berkeley National Laboratories with 180 1° oscillations for all crystals. Data were processed using Mosflm,[31] and for both complexes data from two crystals were merged to improve the completeness (Table 1). Both crystals have one molecule in the asymmetric unit and a solvent content of 57%.

The LC8-QT1p and LC8-QT4p peptide structures were solved at resolutions of 1.3 and 1.6 Å, respectively, by molecular replacement using PHENIX AutoMR[32] with apo-LC8 (PDB 3BRI) as the search model. The resulting $F_o–F_c$ map showed clear density for bound peptide, confirming the molecular replacement solution. Models for bound QT1p and QT4p were constructed using the LC8-Swa complex (PDB 3E2B) as a template. With 10% of the data set aside for cross-validation, the models were subjected to iterative refinement using Coot[33] and phenix.refine,[32] including TLS refinement;[34] ordered water molecules were added using the criteria of having reasonable hydrogen bonding partners and a peak in the $2F_o–F_c$ electron density map of at least 1σ. For the bound peptides, side chain atoms were included for all of the residues that were modeled, even if there was minimal or no density for some of the side chain atoms.

PDB and BMRB Accession Codes.

The coordinates of LC8-QT1p and LC8-QT4p have been deposited in the RCSB protein data bank under accession codes 5E0L and 5E0M, respectively. The chemical shifts for $Chica_{410–478}$ have been deposited in the Biological Magnetic Resonance Data Bank under accession code 26684.

Author Manuscript Author Manuscript Author Manuscript Author Manuscript

RESULTS

Solution Properties of Chica$_{410–478}$.

Sequence-based secondary structure prediction of Chica using the PSIPRED algorithm[35] predicts three helical regions (Figure 2, red cylinders), while the rest of the protein, primarily the C-terminal half, is predicted to be disordered coil (Figure 2, teal). Within the disordered region, the segment corresponding to residues 410–478, Chica$_{410–478}$, contains four putative LC8 recognition sites with the canonical TQT recognition motif. On the basis of the position of the TQT triplet in each motif, we assign the LC8 interacting motifs to residues 415–424 (QT1), 433–442 (QT2), 444–453 (QT3), and 466–475 (QT4) (Figure 2, black bars). Sequence alignment of Chica$_{410−478}$ from nine mammals and one reptile shows high but not perfect conservation of the TQT sites (Figure 2, green).

Recombinant Chica$_{410–478}$ structure is in agreement with the predicted disorder; its ^{15}N HSQC spectrum (Figure 3a) has a pronounced lack of amide proton chemical shift dispersion, and the CD spectrum shows limited ellipticity at 220 nm and a large negative ellipticity at 200 nm (Figure 3b). Resonance assignments were obtained for all residues (Figure 3a). Secondary chemical shifts indicate some weak β-strand character for residues within QT1 and the linker separating QT3 and QT4, but no apparent secondary structure preference in the rest of the sequence (Figure 3c).

To provide insight into the local dynamics of specific segments within Chica$_{410–478}$, ^{15}N longitudinal (T_1), transverse (T_2), and ^{1}H–^{15}N heteronuclear NOE relaxation parameters were measured. A plot of T_2:T_1 ratios versus residue number suggests motional heterogeneity (Figure 3d). T_2/T_1 values range from 0.53 to 0.96, with an average value of 0.62 (dotted line), with the lowest for residues in the linker separating QT3 and QT4, suggesting motional restriction in this region associated with a tendency to form transient structure. Measured heteronuclear NOE values at 15 °C are all zero, as no peaks were detected in the NOE subspectrum, except for the C-terminal residue 478, which has a value of −0.3 (data not shown). We conclude that in this disordered segment, there are regions of transient structure in the linker between QT3 and QT4 inferred from the combination of β-sheet propensity from secondary chemical shifts and restricted dynamics.

Binding of LC8 to Chica$_{410–478}$.

ITC experiments (Figure 4a and Table 1) show that LC8 binds Chica$_{410–478}$ with a K_d of 0.4 μM and a stoichiometry of 3:1 indicating that, consistent with earlier mutagenesis studies,[22] only three of the TQT recognition motifs bind LC8. NMR titration studies to identify which motifs bind were unsuccessful due to limited solubility of the complex at increasing LC8 concentrations. To determine the relative affinities of the recognition motifs, we synthesized corresponding short peptides QT1p, QT2p, QT3p, and QT4p and measured their binding to LC8 by ITC (Figure 4b–d and Table 1). LC8 interacts with QT1p with a dissociation constant of 0.4 μM, identical to the affinity of the full-length segment, while QT2p and QT4p bind to LC8 with over 10-fold weaker affinity with K_d values of 6.3 and 5.2 μM, respectively (Figure 4c,e). The interaction with QT3p is too weak to be measured accurately by ITC (Figure 4d). Interestingly, the thermodynamic parameters of QT1p and Chica$_{410–478}$

Author Manuscript Author Manuscript Author Manuscript Author Manuscript

are very similar; both show favorable binding entropy compared to QT2p and QT4p (Table 1), implying that the interaction of LC8 with QT1 is the dominant binding reaction in the full-length construct. The $T\Delta S$ terms are of opposite sign for QT1p versus QT2p and QT4p, resulting in more than an order of magnitude higher affinity constant for QT1p, even though the ΔH term is more favorable for QT2p and QT4p binding.

Crystal Structures of LC8-Chica Motif Complexes.

To elucidate the molecular determinants of the LC8-Chica interaction, crystal structures of QT1p and QT4p in complex with LC8 were solved. QT1p and QT4p were chosen because they bracket the range of binding thermodynamics and affinities (Table 1). Although the complexes were crystallized under different conditions (see Materials and Methods), the crystal forms are isomorphous and contain one LC8 monomer and peptide in the unit cell. After facile solution by molecular replacement, refinements led to a LC8-QT1p complex at 1.3 Å resolution with R/R_{free} values of 19.6%/20.2%, and a LC8-QT4p complex at 1.6 Å with R/R_{free} values of 20.7%/23.2% (Table 2).

Both peptides bind to LC8 in a similar, extended conformation (Figure 5) in keeping with previously reported crystal structures of LC8 with bound partner peptides. The conserved TQT portions of QT1p and QT4p show identical hydrogen bonding interactions with LC8 and identical buried water molecules (Figure 5b,c). Both structures also highlight similar electrostatic interactions between a side chain carboxylate at position 2 (Glu424 in QT1p or Asp475 in QT4p) and Lys9 of LC8.

Structural Differences Between LC8-QT1p and LC8-QT4p.

The most obvious difference between LC8-QT1p and LC8-QT4p complexes is that the well-defined electron density in QT1p extends the ordered β-strand by two residues compared to QT4p (Figure 6a), implying a high degree of disorder in the N-terminal residues of LC8-QT4p. The last five residues overlay well in the LC8 binding groove with a backbone RMSD of 0.19 Å (Figure 5a). Two notable differences localized to the N-terminal half of the peptide are consistent with differences in QT1p and QT4p binding affinities. The first is at position −3, where a threonine (Thr470) in QT4p substitutes for an alanine in QT1p. Thr470 does not fit the LC8 binding pocket as well and, relative to Ala419, the peptide backbone of Thr470 is pushed out ~0.9 Å at the Cα atoms (Figure 6b). This distorts the hydrogen bonding geometry at three locations: between Thr470O and Val66N, Ser469O and a water molecule, and Thr471N and a water molecule (Figure 6b, pink arrows). The perturbed hydrogen bond geometry and altered packing of Thr470 backbone atoms could contribute to the lower binding affinity of QT4p. At position −4, both the QT4p Ser469 side chain oxygen and the QT1p Asp418 side chain oxygen hydrogen bond with the side chain oxygen of Thr67 (Figure 5b).

The second difference is the presence of Arg468 at position −5 in QT4p. In QT1p, a buried Ile occupies this position. A Val or Ile in the −5 position has been proposed to be an important determinant of binding affinity both by its observed packing against the imidazole group of LC8 His68[3] and by a pepscan analysis showing that Val or Ile at the −5 position enhances binding.[36] Although a buried Arg at position −5 is presumably destabilizing

Author Manuscript Author Manuscript Author Manuscript Author Manuscript

compared to an Ile or Val, it appears to be acceptable at this position due to a stabilizing cation-π interaction that it makes with Phe73.

DISCUSSION

Chica Motifs Span the Range of LC8 Affinity.

Although LC8 sequences are highly conserved (94% identity between Drosophila and human, and 100% between rat/mice and human), the LC8 recognition motifs carried on LC8 partners are rather variable in sequence except for the TQT consensus triplet. Equally variable is motif affinity for LC8. Full answers to pressing questions of LC8 biological function remain elusive, and the adaptive function of LC8 motif diversity is unknown. One approach is to ask how, at the molecular level, LC8 accommodates so many motif sequences and apply the answers to development of predictive principles for identifying new LC8 partners. In experiments directed toward these general goals, we analyze the structural biology of LC8-Chica interactions to elucidate features that guide LC8-motif recognition.

Among multiple LC8-binding partners (Figure 7), some have TQT motifs of varying LC8 affinity, and a few have TQT motifs that do not bind LC8 at all. The protein studied here, human Chica, contains four potential LC8 recognition motifs, out of which three bind LC8. Spectroscopic measurements confirm that $Chica_{410–478}$ is intrinsically disordered as predicted from sequence (Figure 3), and calorimetric studies show that it binds three LC8 molecules (Figure 4 and Table 1), as expected from previous reports.[22] Affinities of the TQT motifs, determined by calorimetric experiments with synthetic 14-amino acid peptides corresponding to each of the four motifs, vary from 0.4 μM for QT1p to immeasurably weak for QT3p (Table 1). In this single protein, the affinities of LC8-binding sequences span the range of LC8 recognition motifs, from 0.16 μM for Nek9[16] to 42.7 μM for Pak1.[19] Thus, Chica is an ideal model system for studying the molecular bases of TQT motif recognition by LC8.

Why Multiple Motifs?

While it is not clear at this stage why some LC8 partner proteins are multivalent, it is clear that they are numerous and biologically diverse, and that their LC8-recognition sites are present exclusively in intrinsically disordered segments of the partner (Figure 7). For some LC8 partners with multiple binding sites, various functions of the multiplicity have been proposed. In Nup159, the multiple sites act cooperatively so that binding of the first LC8 enhances binding of the next,[23] and apparently contributes to the stability of the complex. Electron microscopic studies of nuclear pore assembly suggest that incorporation of Nup159 into the nuclear pore does not occur until all LC8 sites are filled.[37,38] In ASCIZ, the multiple motifs could act as a sensor for LC8 cellular concentration.[9] ASCIZ is an LC8 transcription factor, and it is possible that the level of bound LC8 could modulate its LC8-dependent transcription activity. In Ana2, binding of two LC8 dimers promotes self-aggregation of Ana2 into a tetramer, possibly by aiding formation of a coiled-coil region located between the two binding sites.[14] In Pac11, two LC8 sites flank a nascent helix which forms a self-associated helix/helix interface upon LC8 binding.[39]

Author Manuscript Author Manuscript Author Manuscript Author Manuscript

In Chica, the lack of LC8 binding to QT3 is consistent with its lower conservation. Out of the four TQT motifs, QT3 is least conserved: in one species (*Propithecus coquereli*), it has a mutant TQT sequence and in another (*Eptesicus fuscus*) it is missing entirely (Figure 2). The stability of the LC8/Chica$_{410–478}$ complex containing three LC8 molecules (average binding affinity) is the same as for LC8/QT1p, suggesting that the role of the other motifs is not for forming a stable complex. One possibility for the Chica/LC8 assembly is that QT1/LC8 binding initiates the process and later QT2/LC8 and QT4/LC8 binding promote self-association, perhaps in QT3 and the linker separating QT2 and QT4 similar to that observed with Ana2 and Pac11. This proposal is consistent with secondary structure propensity in the linker separating QT3 and QT4 in free Chica indicated by secondary chemical shifts and restricted dynamics (Figure 3c,d).

The Crystal Structures of LC8/Chica Motifs Distinguish Two Regions of Interactions.

In LC8-QT1p and LC8-QT4p, the TQT residues of the peptide interact with the same LC8 atoms in a network of polar interactions involving buried atoms in both backbone and side chains, as shown in Figure 5b,c. LC8 residues in the TQT network are 62–64 at the N-terminus of β3 strand and residues 35′ and 36′ in the α2 helix of the other LC8 monomeric unit. Three-dimensional positions of every atom in this region of the LC8/motif binding site overlay well in both complexes, with an RMS deviation of 0.25 Å.

In non-TQT regions of LC8/motif binding sites, the correlation of motif position with affinity is highly complex. For example, the main chain conformation of QT4p (Figure 6b, green) is different from QT1p (orange) at T$_{-3}$, resulting in QT4p H-bonding geometry that appears to be less favorable (pink arrows). This is expected to lower affinity, but the actual affinity of QT4 relative to QT1 peptides cannot be ascribed to this effect alone, or even primarily, because there are many other amino acid differences at non-TQT positions, some of which lead to the degree of disorder of positions −6 and −7 in QT4. As a second example of the complexity of correlating affinity with sequence, the sequences of QT2 and QT4 are different at every position outside of the TQT (Figure 2), but they bind LC8 with a similar affinity (Table 1).

Similarly, it is tempting to expect that QT2 should have lower affinity than QT1, as QT2 lacks the stabilizing electrostatic interactions at position 2 (Glu– > Ser) and the long hydrophobic side chain at position −5 (Ile– > Ser). However, other non-TQT positions are different as well, and how the contributions of amino acids at individual positions give the overall affinity is not clear. That is, an a priori sequence-based prediction of relative affinity of two motifs, or even prediction of whether a motif binds at all, is not feasible. A further illustration of this complexity comes from a comparison of Chica QT3 which essentially does not bind LC8, to Ana2 QT1 which has a binding affinity of 1.1 μM.[14] Between Chica QT3 and Ana2 QT1, the most notable sequence differences are at position 2 (Asp– > Ala), and at position −5 (Ile– > Ala) (Figure 6c). An Asp at position 2 makes a favorable interaction with Lys9 in LC8 and a long hydrophobic side chain is more stabilizing than an Ala at position −5. The combined effect of the two replacements is reasonably assumed to diminish binding. So it is tempting to expect that these two substitutions together could suggest a position “rule” for predicting whether TQT motifs in fact bind LC8, especially

Author Manuscript Author Manuscript Author Manuscript Author Manuscript

since Chica QT1 and Ana2 QT1 both have Ile at position −5 and a carboxyl side chains at position 2. But, even this simple correlation does not hold up, because QT2 has Ser at both −5 and 2, and it still binds better than QT3.

In summary, analyses of Chica motif complexes with LC8, and of other LC8-peptide crystal structures (Figure 8), support the generalization that there are two functionally distinct parts of the LC8-motif binding site: the TQT residues are the main determinant of motif sequence specificity and the non-TQT residues modulate overall LC8-motif affinity and provide finely tuned association/dissociation constants for selection by LC8. In the TQT region, LC8/TQT interactions are invariant and highly constrained. In contrast, the LC8/non-TQT interactions are highly variable, and their contributions to binding stability are complex and interdependent. We suggest the term “anchored flexibility” to capture the manner in which LC8/motif sequence specificity resides primarily in LC8/TQT interactions and affinity modulation resides in LC8/non-TQT interactions.

Molecular Determinants of LC8 Recognition: The “Anchored Flexibility” Model.

Flexibility of LC8 partners is inherent to the intrinsic disorder first noted as their distinguishing feature,[2] and flexibility and shear movement of the LC8 binding groove were proposed as a basis for the wide variability in motif sequence and binding affinity.[12,40–42] To the concept of groove flexibility, we add the feature of a TQT “anchor” within one binding site that in other regions is dynamic.

As the LC8/Chica motif complexes illustrate (Figure 5), the “anchor” region of the LC8 binding site engages peptide TQT residues in a network of polar interactions involving buried H-bond donors and acceptors in both LC8 subunits. Such a buried network requires optimal H-bonding geometry, the distortion of which is energetically costly, especially in an apolar milieu. The TQT region of the LC8-motif complex is highly ordered and rigidly packed (anchored) compared to the other more flexible motif positions (2, −2 to −7). The plasticity of the non-TQT regions of the complex is reflected in the conformational accommodation of numerous sequence permutations with similarly variable affinities. The flexibility resides in non-TQT residues and LC8 residues that bind them, while the anchor is composed of TQT residues and LC8 residues 35′, 36′, and 62–64. It is likely that these features underlie the evolutionary fitness of LC8-motif interactions.

Structural parameters of the two complexes of Chica motif peptides with LC8 (Figures 5 and 6a) and other LC8-peptide complexes (Figure 8) support the anchored flexibility model. If TQT-LC8 interacting residues are more rigid and tightly packed than other motif residues, then they should have smaller *B*-factors and low solvent accessibility in crystal structures of LC8-peptide complexes. A comparison of the *B*-factors of LC8-QT1p and LC8-QT4p (Figure 6d) upholds the expected correlation. For QT1p backbone (orange) and side chains (red), TQT atoms have the lowest *B*-factors in the peptide. Further, in LC8-QT1p and LC8-QT4p, LC8 residues 62–64 bound to TQT have the lowest *B*-factors in the complex (data not shown). In apo LC8, *B*-factors of residues 62–64 are among the lowest,[40] suggesting that a high degree of order in unbound LC8 minimizes the unfavorable entropy loss associated with rigid binding of the TQT anchor. The same trend of TQT residues exhibiting

Author Manuscript Author Manuscript Author Manuscript Author Manuscript

significantly lower *B*-factors than residues at other positions is observed in all available LC8-peptide complex structures (Figure 8a).

An analysis of the solvent accessible surface areas of nine LC8-peptide structures shows a similar backbone solvent accessibility profile among all peptides for residues at positions −6 to 2 (Figure 8b, top). The alternating high/low solvent accessibility pattern is consistent with the elongated β-strand structure of the peptide and shows that all peptides, regardless of their binding affinities, form a strand at these positions. The TQT “anchor” has complete burial of side chains in the LC8 binding pocket at positions −1 to 1, even for non-threonine side chains (Figure 8b, bottom). Solvent accessibility for side chains at other positions varies considerably, demonstrating the higher flexibility of the non-TQT regions of the peptide binding groove.

The model does not require that all non-TQT positions are equally variable, and the motif logo in Figure 1b demonstrates amino acid preferences at some non-TQT positions. Because the non-TQT peptide residues and associated LC8 residues are flexible in the complex, destabilizing energetic effects of an unfavorable contact introduced by a specific mutation may be readily compensated by numerous small, stabilizing conformational adjustments. Strain and unfavorable contacts are eased by relaxation processes of equilibrating conformations so that numerous sequence permutations are accommodated in the non-TQT regions of the binding site. Still, the positions adjacent to TQT (−2 and 2) are more constrained than other positions due to their proximity to TQT, and residue preference at these positions should be higher than for others, as observed especially for position 2 (logo, Figure 1) where the Asp side chain interacts with Lys9 of LC8.

In summary, the anchored flexibility model explains the requirement for the TQT triplet and the ability of LC8 grooves to accommodate numerous sequence permutations outside the TQT. Simple rules of position-dependent affinity effects are, at our present level of knowledge, ineffective in predicting new additions to the LC8 interactome from motif sequence. Given this, we suggest that predictive algorithms for identifying new LC8 binding partners should be based on statistical position preferences which await identification of binding affinities of a large number of binding motifs.

ACKNOWLEDGMENTS

The authors wish to thank Prof. Clare Woodward and the Barbar lab for valuable discussions.

Funding

This work was supported by National Institutes of Health Grant GM 084276 to E.B. Support to facilities includes NIH/NIEHS 00210 for the protein core facility in the OSU Environmental Health Sciences Center, and the seventh Framework Programme of the EC (Project Number: 261863, Bio-NMR) (Frankfurt, Germany).

ABBREVIATIONS

Ana2
anastral spindle-2

ASCIZ

Author Manuscript Author Manuscript Author Manuscript Author Manuscript

ATM-substrate Chk-interacting Zn^{2+} finger

QT1p, QT2p, QT3p, and QT4p

peptides corresponding to recognition motifs 1–4, respectively

ITC

isothermal titration calorimetry

REFERENCES

(1). King SM, Barbarese E, Dillman JF, PatelKing RS, Carson JH, and Pfister KK (1996) Brain cytoplasmic and flagellar outer arm dyneins share a highly conserved M(r) 8,000 light chain. J. Biol. Chem 271, 19358–19366. [PubMed: 8702622]

(2). Barbar E (2008) Dynein light chain LC8 is a dimerization hub essential in diverse protein networks. Biochemistry 47, 503–508. [PubMed: 18092820]

(3). Rapali P, Radnai L, Suveges D, Harmat V, Tolgyesi F, Wahlgren WY, Katona G, Nyitray L, and Pal G (2011) Directed evolution reveals the binding motif preference of the LC8/DYNLL hub protein and predicts large numbers of novel binders in the human proteome. PLoS One 6, e18818. [PubMed: 21533121]

(4). Barbar E, and Nyarko A (2014) NMR Characterization of Self-Association Domains Promoted by Interactions with LC8 Hub Protein. Comput. Struct. Biotechnol. J 9, e201402003. [PubMed: 24757501]

(5). Lo KW, Kan HM, Chan LN, Xu WG, Wang KP, Wu Z, Sheng M, and Zhang M (2005) The 8-kDa dynein light chain binds to p53-binding protein 1 and mediates DNA damage-induced p53 nuclear accumulation. J. Biol. Chem 280, 8172–8179. [PubMed: 15611139]

(6). Rayala SK, den Hollander P, Manavathi B, Talukder AH, Song C, Peng S, Barnekow A, Kremerskothen J, and Kumar R (2006) Essential role of KIBRA in co-activator function of dynein light chain 1 in mammalian cells. J. Biol. Chem 281, 19092–19099. [PubMed: 16684779]

(7). Poisson N, Real E, Gaudin Y, Vaney MC, King S, Jacob Y, Tordo N, and Blondel D (2001) Molecular basis for the interaction between rabies virus phosphoprotein P and the dynein light chain LC8: dissociation of dynein-binding properties and transcriptional functionality of P. J. Gen. Virol 82, 2691–2696. [PubMed: 11602781]

(8). Kubota T, Matsuoka M, Chang TH, Bray M, Jones S, Tashiro M, Kato A, and Ozato K (2009) Ebolavirus VP35 interacts with the cytoplasmic dynein light chain 8. J. Virol 83, 6952–6956. [PubMed: 19403681]

(9). Jurado S, Conlan LA, Baker EK, Ng JL, Tenis N, Hoch NC, Gleeson K, Smeets M, Izon D, and Heierhorst J (2012) ATM substrate Chk2-interacting Zn2+ finger (ASCIZ) Is a bi-functional transcriptional activator and feedback sensor in the regulation of dynein light chain (DYNLL1) expression. J. Biol. Chem 287, 3156–3164. [PubMed: 22167198]

(10). Barbar E, Kleinman B, Imhoff D, Li MG, Hays TS, and Hare M (2001) Dimerization and folding of LC8, a highly conserved light chain of cytoplasmic dynein. Biochemistry 40, 1596–1605. [PubMed: 11327818]

(11). Clark SA, Jespersen N, Woodward C, and Barbar E (2015) Multivalent IDP assemblies: Unique properties of LC8-associated, IDP duplex scaffolds. FEBS Lett. 589, 2543–2551. [PubMed: 26226419]

(12). Benison G, Karplus PA, and Barbar E (2007) Structure and dynamics of LC8 complexes with KXTQT-motif peptides: swallow and dynein intermediate chain compete for a common site. J. Mol. Biol 371, 457–468. [PubMed: 17570393]

(13). Liang J, Jaffrey SR, Guo W, Snyder SH, and Clardy J (1999) Structure of the PIN/LC8 dimer with a bound peptide. Nat. Struct Mol. Biol 272, 20929–20935.

(14). Slevin LK, Romes EM, Dandulakis MG, and Slep KC (2014) The Mechanism of Dynein Light Chain LC8-mediated Oligomerization of the Ana2 Centriole Duplication Factor. J. Biol. Chem 289, 20727–20739. [PubMed: 24920673]

Author Manuscript Author Manuscript Author Manuscript Author Manuscript

(15). Rao L, Romes EM, Nicholas MP, Brenner S, Tripathy A, Gennerich A, and Slep KC (2013) The yeast dynein Dyn2-Pac11 complex is a dynein dimerization/processivity factor: structural and single-molecule characterization. Mol. Biol. Cell 24, 2362–2377. [PubMed: 23761070]

(16). Gallego P, Velazquez-Campoy A, Regue L, Roig J, and Reverter D (2013) Structural analysis of the regulation of the DYNLL/LC8 binding to Nek9 by phosphorylation. J. Biol. Chem 288, 12283–12294. [PubMed: 23482567]

(17). Bodor A, Radnai L, Hetenyi C, Rapali P, Lang A, Kover KE, Perczel A, Wahlgren WY, Katona G, and Nyitray L (2014) DYNLL2 dynin light chain binds to an extended linear motif of myosin 5a tail that has structural plasticity. Biochemistry 53, 7107–7122. [PubMed: 25312846]

(18). Romes EM, Tripathy A, and Slep KC (2012) Structure of a yeast Dyn2-Nup159 complex and molecular basis for dynein light chain-nuclear pore interaction. J. Biol. Chem 287, 15862–15873. [PubMed: 22411995]

(19). Lightcap CM, Sun S, Lear JD, Rodeck U, Polenova T, and Williams JC (2008) Biochemical and structural characterization of the Pak1-LC8 interaction. J. Biol. Chem 283, 27314–27324. [PubMed: 18650427]

(20). Wagner W, Fodor E, Ginsburg A, and Hammer JA 3rd (2006) The binding of DYNLL2 to myosin Va requires alternatively spliced exon B and stabilizes a portion of the myosin's coiled-coil domain. Biochemistry 45, 11564–11577. [PubMed: 16981716]

(21). Nyarko A, Hall J, Hall A, Hare M, Kremerskothen J, and Barbar E (2011) Conformational dynamics promote binding diversity of dynein light chain LC8. Biophys. Chem 159, 41–47. [PubMed: 21621319]

(22). Dunsch AK, Hammond D, Lloyd J, Schermelleh L, Gruneberg U, and Barr FA (2012) Dynein light chain 1 and a spindle-associated adaptor promote dynein asymmetry and spindle orientation. J. Cell Biol 198, 1039–1054. [PubMed: 22965910]

(23). Nyarko A, Song Y, Novacek J, Zidek L, and Barbar E (2013) Multiple recognition motifs in nucleoporin Nup159 provide a stable and rigid Nup159-Dyn2 assembly. J. Biol. Chem 288, 2614–2622. [PubMed: 23223634]

(24). Rapali P, Garcia-Mayoral MF, Martinez-Moreno M, Tarnok K, Schlett K, Albar JP, Bruix M, Nyitray L, and Rodriguez-Crespo I (2011) LC8 dynin light chain (DYNLL1) binds to the C-terminal domain of ATM-interacting protein (ATMIN/ASCIZ) and regulates its subcellular localization. Biochem. Biophys. Res. Commun 414, 493–498. [PubMed: 21971545]

(25). Favier A, and Brutscher B (2011) Recovering lost magnetization: polarization enhancement in biomolecular NMR. J. Biomol. NMR 49, 9–15. [PubMed: 21190063]

(26). Lescop E, Kern T, and Brutscher B (2010) Guidelines for the use of band-selective radiofrequency pulses in hetero-nuclear NMR: example of longitudinal-relaxation-enhanced BEST-type 1H-15N correlation experiments. J. Magn. Reson 203, 190–198. [PubMed: 20031460]

(27). Johnson BA, and Blevins RA (1994) NMRView: A computer program for visualization and analysis of NMR data. J. Biomol. NMR 4, 603–614. [PubMed: 22911360]

(28). Ferrage F, Piserchio A, Cowburn D, and Ghose R (2008) On the measurement of 15N-{1H} nuclear Overhauser effects. J. Magn. Reson 192, 302–313. [PubMed: 18417394]

(29). Lakomek NA, Ying J, and Bax A (2012) Measurement of (1) (5)N relaxation rates in perdeuterated proteins by TROSY-based methods. J. Biomol. NMR 53, 209–221. [PubMed: 22689066]

(30). Goddard TD, and Kneller DG SPARKY 3, San Francisco, California.

(31). Leslie AGW, and Powell HR (2007) Processing Diffraction Data with Mosflm. Evolving Methods Macromol. Crystallogr 245, 41–51.

(32). Adams PD, Afonine PV, Bunkoczi G, Chen VB, Davis IW, Echols N, Headd JJ, Hung LW, Kapral GJ, Grosse-Kunstleve RW, McCoy AJ, Moriarty NW, Oeffner R, Read RJ, Richardson DC, Richardson JS, Terwilliger TC, and Zwart PH (2010) PHENIX: a comprehensive Python-based system for macromolecular structure solution. Acta Crystallogr., Sect. D: Biol. Crystallogr 66, 213–221. [PubMed: 20124702]

(33). Emsley P, Lohkamp B, Scott WG, and Cowtan K (2010) Features and development of Coot. Acta Crystallogr., Sect. D: Biol. Crystallogr 66, 486–501. [PubMed: 20383002]

Author Manuscript Author Manuscript Author Manuscript Author Manuscript

(34). Winn MD, Isupov MN, and Murshudov GN (2001) Use of TLS parameters to model anisotropic displacements in macromolecular refinement. Acta Crystallogr., Sect. D: Biol. Crystallogr 57, 122–133. [PubMed: 11134934]

(35). McGuffin LJ, Bryson K, and Jones DT (2000) The PSIPRED protein structure prediction server. Bioinformatics 16, 404–405. [PubMed: 10869041]

(36). Lajoix AD, Gross R, Aknin C, Dietz S, Granier C, and Laune D (2004) Cellulose membrane supported peptide arrays for deciphering protein-protein interaction sites: the case of PIN, a protein with multiple natural partners. Mol. Diversity 8, 281–290.

(37). Stelter P, Kunze R, Radwan M, Thomson E, Thierbach K, Thoms M, and Hurt E (2012) Monitoring spatiotemporal biogenesis of macromolecular assemblies by pulse-chase epitope labeling. Mol. Cell 47, 788–796. [PubMed: 22819325]

(38). Gaik M, Flemming D, von Appen A, Kastritis P, Mucke N, Fischer J, Stelter P, Ori A, Bui KH, Bassler J, Barbar E, Beck M, and Hurt E (2015) Structural basis for assembly and function of the Nup82 complex in the nuclear pore scaffold. J. Cell Biol. 208, 283–297. [PubMed: 25646085]

(39). Jie J, Lohr F, and Barbar E (2015) Interactions of yeast dynein with dynein light chain and dynactin: General implications for intrinsically disordered duplex scaffolds in multi-protein assemblies. J. Biol. Chem 290, 23863. [PubMed: 26253171]

(40). Benison G, Karplus PA, and Barbar E (2008) The Interplay of Ligand Binding and Quaternary Structure in the Diverse Interactions of Dynein Light Chain LC8. J. Mol. Biol 384, 954–966. [PubMed: 18948118]

(41). Hall J, Hall A, Pursifull N, and Barbar E (2008) Differences in dynamic structure of LC8 monomer, dimer, and dimer-peptide complexes. Biochemistry 47, 11940–11952. [PubMed: 18942858]

(42). Fan JS, Zhang Q, Tochio H, and Zhang M (2002) Backbone dynamics of the 8 kDa dynein light chain dimer reveals molecular basis of the protein's functional diversity. J. Biomol. NMR 23, 103–114. [PubMed: 12153036]

(43). Kjaergaard M, Brander S, and Poulsen FM (2011) Random coil chemical shift for intrinsically disordered proteins: effects of temperature and pH. J. Biomol. NMR 49, 139–149. [PubMed: 21234644]

(44). Winn MD, Ballard CC, Cowtan KD, Dodson EJ, Emsley P, Evans PR, Keegan RM, Krissinel EB, Leslie AG, McCoy A, McNicholas SJ, Murshudov GN, Pannu NS, Potterton EA, Powell HR, Read RJ, Vagin A, and Wilson KS (2011) Overview of the CCP4 suite and current developments. Acta Crystallogr., Sect. D: Biol. Crystallogr 67, 235–242. [PubMed: 21460441]

(45). McDonnell AV, Jiang T, Keating AE, and Berger B (2006) Paircoil2: improved prediction of coiled coils from sequence. Bioinformatics 22, 356–358. [PubMed: 16317077]

(46). Fejtova A, Davydova D, Bischof F, Lazarevic V, Altrock WD, Romorini S, Schone C, Zuschratter W, Kreutz MR, Garner CC, Ziv NE, and Gundelfinger ED (2009) Dynein light chain regulates axonal trafficking and synaptic levels of Bassoon. J. Cell Biol 185, 341–355. [PubMed: 19380881]

(47). Rodriguez-Crespo I, Yelamos B, Roncal F, Albar JP, Ortiz de Montellano PR, and Gavilanes F (2001) Identification of novel cellular proteins that bind to the LC8 dynin light chain using a pepscan technique. FEBS Lett. 503, 135–141. [PubMed: 11513870]

(48). Hall J, Karplus PA, and Barbar E (2009) Multivalency in the assembly of intrinsically disordered dynein intermediate chain. J. Biol. Chem 284, 33115–33121. [PubMed: 19759397]

(49). Gupta A, Diener DR, Sivadas P, Rosenbaum JL, and Yang P (2012) The versatile molecular complex component LC8 promotes several distinct steps of flagellar assembly. J. Cell Biol. 198, 115–126. [PubMed: 22753897]

(50). Zaytseva O, Tenis N, Mitchell N, Kanno S, Yasui A, Heierhorst J, and Quinn LM (2014) The novel zinc finger protein dASCIZ regulates mitosis in Drosophila via an essential role in dynein light-chain expression. Genetics 196, 443–453. [PubMed: 24336747]

(51). Fraczkiewicz R, and Braun W (1998) Exact and Efficient Analytical Calculation of the Accessible Surface Areas and Their Gradients for Macromolecules. J. Comput. Chem 19, 319–333.

Author Manuscript Author Manuscript Author Manuscript Author Manuscript

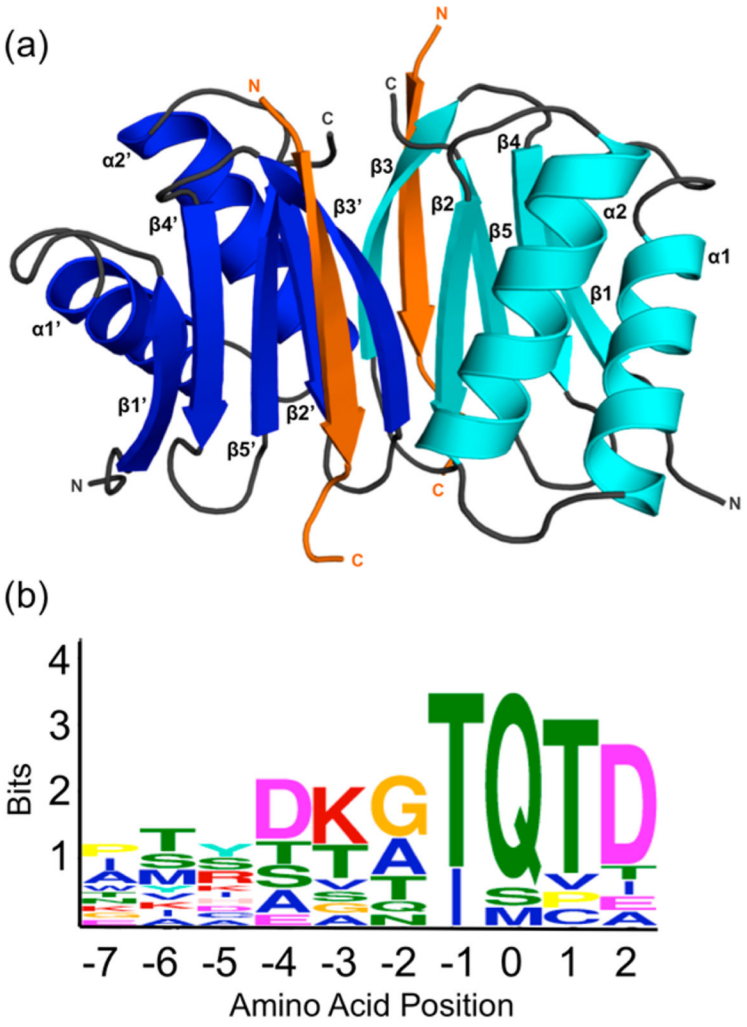

Figure 1.

LC8 binds many partners in symmetrical grooves at its dimer interface. (a) A ribbon diagram of the LC8 dimer (blue and cyan) bound to two chains of the Chica QT1 peptide determined in this study (orange). Structures of all LC8/peptide complexes look essentially the same. LC8 secondary structure elements are labeled. (b) A sequence logo of LC8 binding motifs derived from sequences of the motifs in the 11 crystal structures reported for LC8/peptide complexes. Height of amino acids indicates their relative frequency at that position.

Author Manuscript Author Manuscript Author Manuscript Author Manuscript

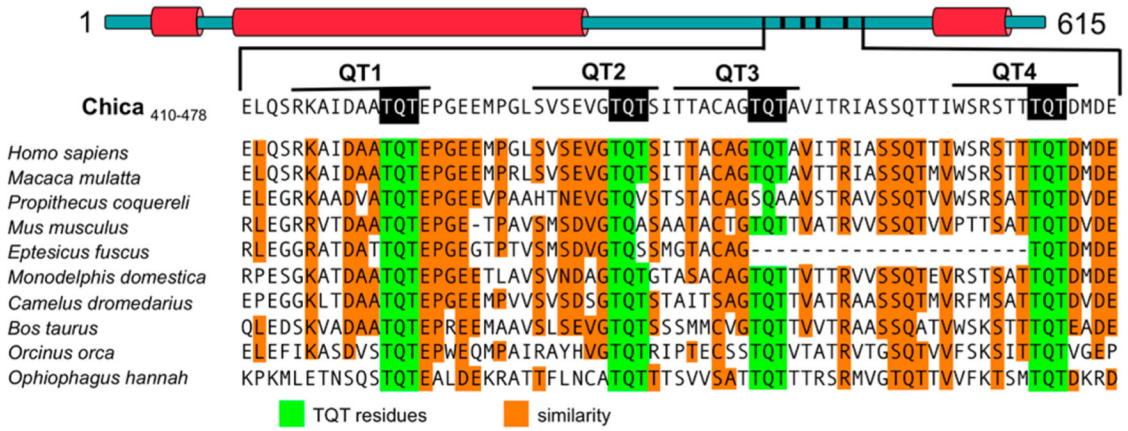

Figure 2.

LC8 binding region of Chica is disordered and conserved. Four putative LC8 binding sites, QT1, QT2, QT3, and QT4 (black highlight), are nestled within a segment of Chica (410–478) predicted to be disordered (teal). Predicted structured regions are shown as red cylinders. Conserved TQT residues in each motif are highlighted in black, and a black bar indicates the full 10-amino acid sequence. A sequence alignment across 10 species is shown below with 100% identity shown in green and similarity shown in orange. Species were chosen to cover a wide genus range; percent sequence identity relative to the *Homo sapiens* sequence ranges from 67 to 96%.

Author Manuscript Author Manuscript Author Manuscript Author Manuscript

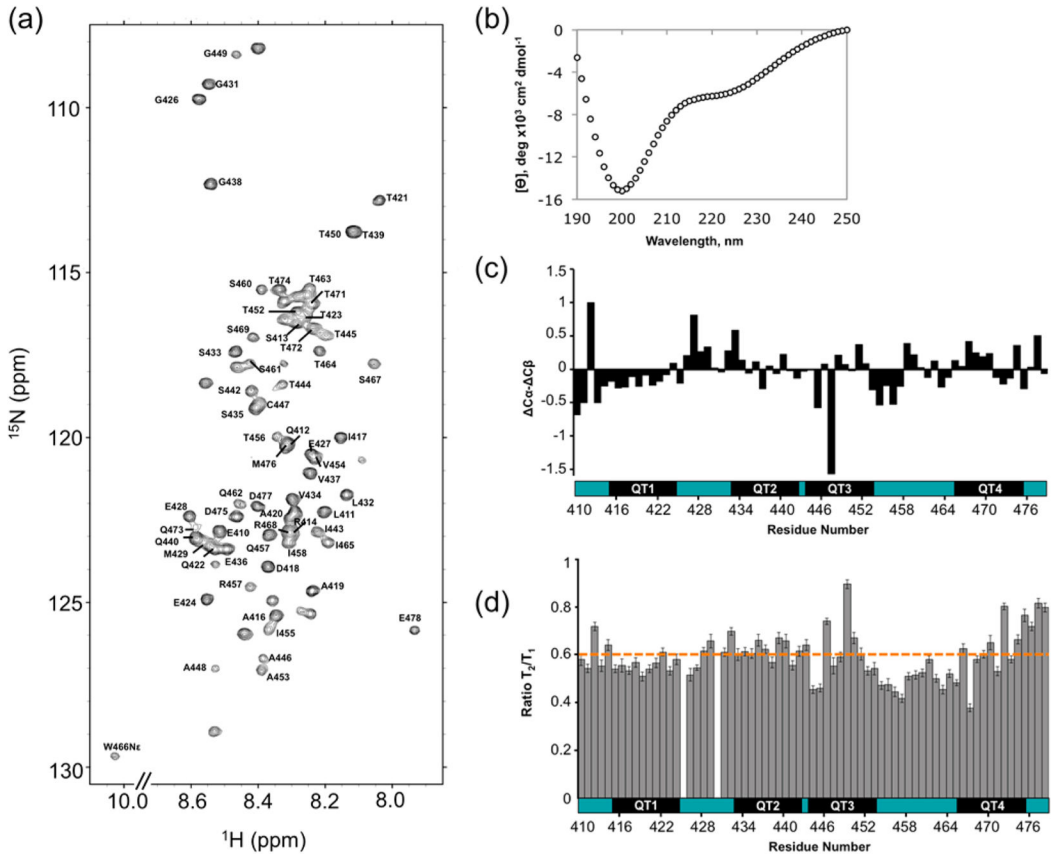

Figure 3.

Spectroscopic analyses of Chica$_{410–478}$. (a) [^{15}N–^{1}H]-BEST-TROSY spectrum showing backbone assignments for all 67 nonproline residues. Unassigned residues correspond to the additional N-terminal residues from the expression vector. The spectrum was recorded at 15 °C. (b) Far UV CD spectrum collected at 25 °C. (c) A plot of chemical shift differences versus residue number. $\Delta C\alpha$ and $\Delta C\beta$ values were calculated by subtracting the random coil chemical shift from the experimentally determined chemical shift value.[43] $\Delta C\alpha - \Delta C\beta$ values > ± 1.0 ppm were considered significant. (d) Plot of T_2/T_1 relaxation per residue. Segments corresponding to recognition motifs, QT1, QT2, QT3, and QT4 are shown below the plot.

Author Manuscript Author Manuscript Author Manuscript Author Manuscript

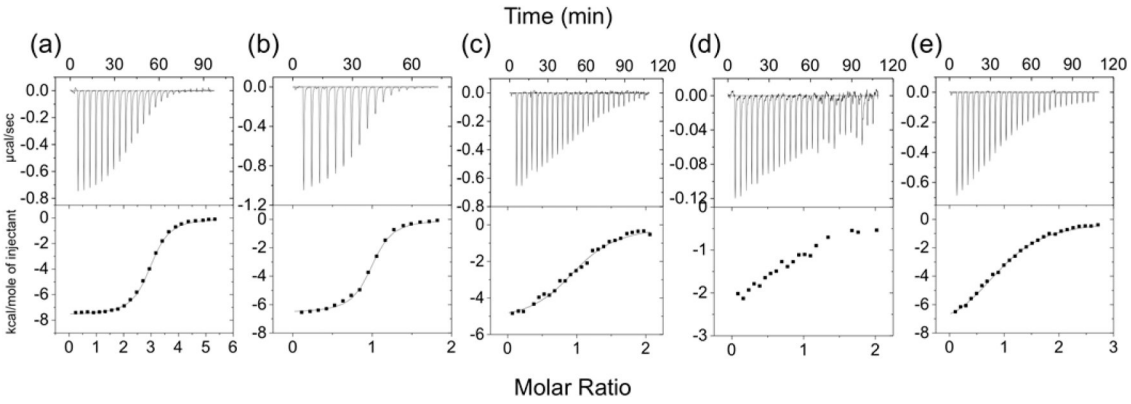

Figure 4.

LC8-Chica interactions monitored by isothermal titration calorimetry. Representative thermograms are shown for the interaction of LC8 with (a) $Chica_{410–478}$, and peptides corresponding to (b) QT1p (c) QT2p, (d) QT3p, and (e) QT4p recognition sequences.

Author Manuscript Author Manuscript Author Manuscript Author Manuscript

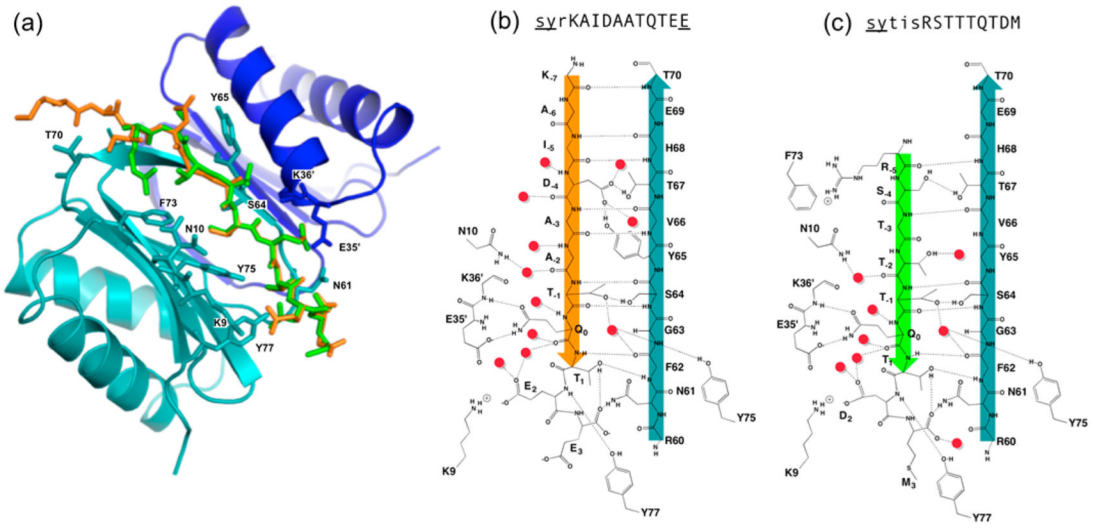

Figure 5.

Comparisons of crystal structures of the LC8-QT1p and LC8-QT4p complexes. (a) Chica peptides QT1p(orange) and QT4p (green) overlaid after alignment of the mainchain residues of their respective LC8 homodimers. The side chains of LC8 residues that form hydrogen bonds or a cation-π interaction (F73) with QT1p or QT4p are shown as sticks and labeled. For the sake of clarity, only one peptide bound to LC8 is shown. A schematic of (b) QT1p (orange) bound to LC8 compared to (c) QT4p (green) bound to LC8 highlights similarities and differences in LC8 residues involved in the hydrogen bonding or stabilizing interactions based upon the peptide sequence. The sequence of each peptide is shown above each diagram with capital letters corresponding to residues that are observed in the crystal structure, while those in small letters are part of the peptide but are not observed and underlined residues are nonnative.

Author Manuscript Author Manuscript Author Manuscript Author Manuscript

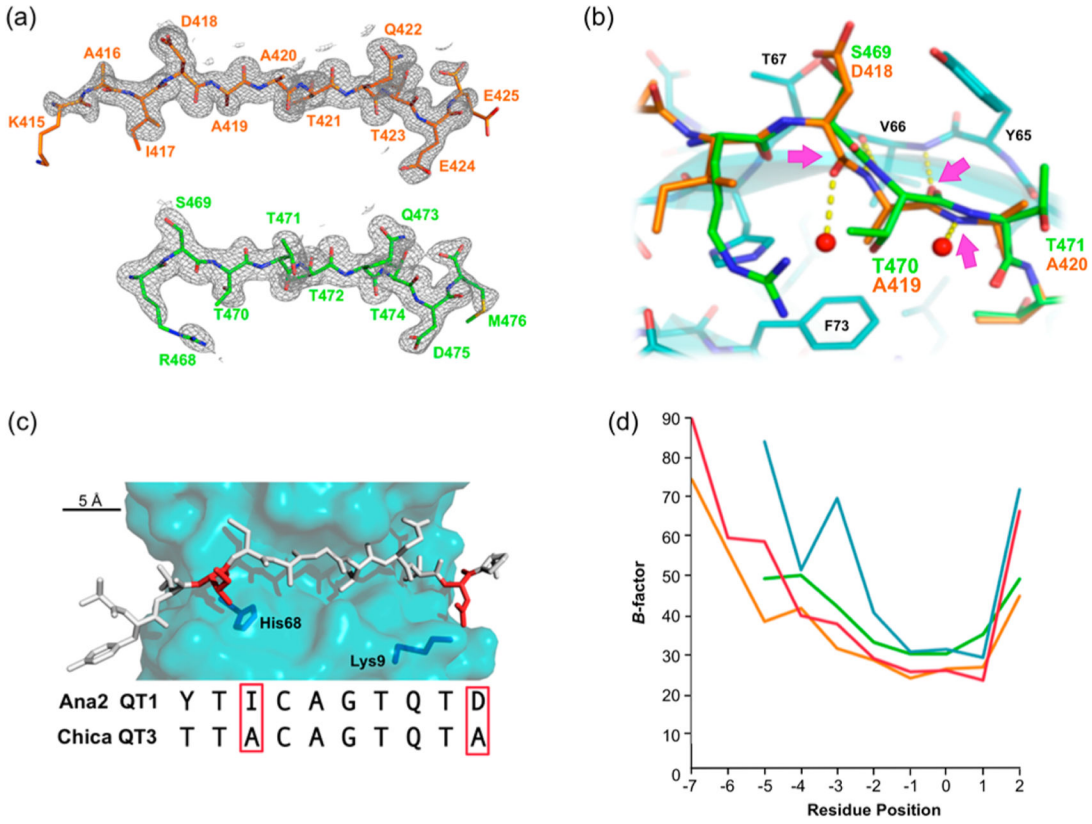

Figure 6.

Crystal structures of motif peptides bound to LC8. (a) The $2F_O–F_C$ electron density for Chica QT1p (top) and Chica QT4p (bottom) is shown as gray mesh, contoured at 1.0σ. (b) The main chain conformation of the QT4p (green) is different from the QT1p (orange) at position −3 (T_{-3}) due to a buried T470 in LC8. QT4p H-bonding geometry is unfavorable at three locations (pink arrows). (c) Ana2 QT1 peptide (PDB 4QH7) is shown in the LC8 binding groove with positions of lysine 9 and histidine 68 labeled. Ana2 QT1 and Chica QT3p peptides have highly similar motifs but very different affinities; the primary sequence differences are shown in red rectangles. (d) The *B*-factors of backbone QT1p atoms (orange), side chain QT1p atoms (red), backbone QT4p atoms (green), and side chain QT4p atoms (blue) are plotted at each residue position. *B*-factors for backbone or side chain atoms were averaged using the program “baverage” available through the CCP4 suite.[44]

Author Manuscript Author Manuscript Author Manuscript Author Manuscript

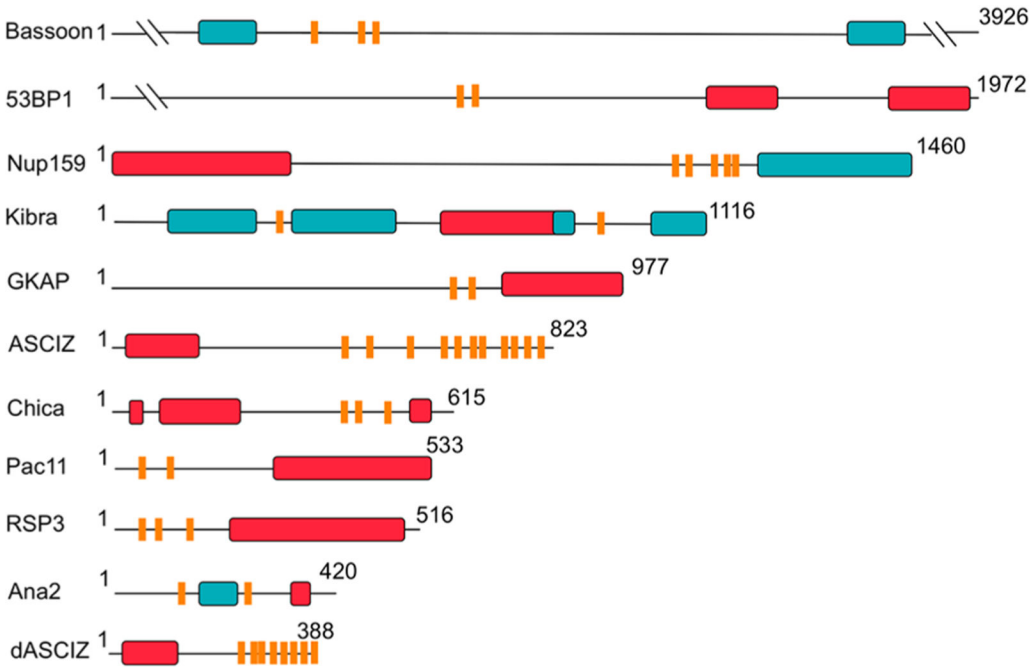

Figure 7.

LC8 binding partners have multiple recognition motifs in intrinsically disordered regions. Sequence-based predictions of order (red boxes), disorder (black lines), coiled-coil (blue boxes), and LC8 binding motifs (orange bars) are shown for residues 1000–2500 of Bassoon, a protein involved in the organization of the cytomatrix at the nerve terminals active zone; residues 500–1972 of p53 binding protein 1 (53BP1), a protein which activates p53-dependent gene transcription; yeast nucleoporin, Nup159, a protein in the nuclear pore complex; Kibra, a protein involved in tissue homeostatis and regulation of organ size; guanylate kinase-associated protein (GKAP), a protein that orchestrates protein remodeling at synapses; DNA damage repair protein and transcription factor ATM-Substrate Chk-interacting zincfinger (ASCIZ); the intermediate chain (Pac11) subunit of the yeast cytoplasmic dynein molecular motor; Chica, a spindle-associated adaptor protein; the flagellar radial spoke protein 3, RSP3; anastral spindle-2 (Ana2), a protein involved in centriole duplication, and the Drosophila homologue of ASCIZ (dASCIZ). Sequence predictions of order and disorder were obtained using the program PSIPRED,[35] where our criteria for structure was based on >10% probability of predicted structure in a 50+ amino acid stretch, and coiled-coils were predicted using the program Paracoil2,[45] where predicted coiled-coils with a p-value <0.025 were considered significant. Putative LC8 binding motifs are based on the following references: bassoon,[46] 53BP1,[5] Nup159,[23] Kibra,[6] GKAP,[47] ASCIZ,[24] IC,[48] Chica,[22] RSP3,[49] Ana2,[14] and dASCIZ.[50]

Author Manuscript Author Manuscript Author Manuscript Author Manuscript

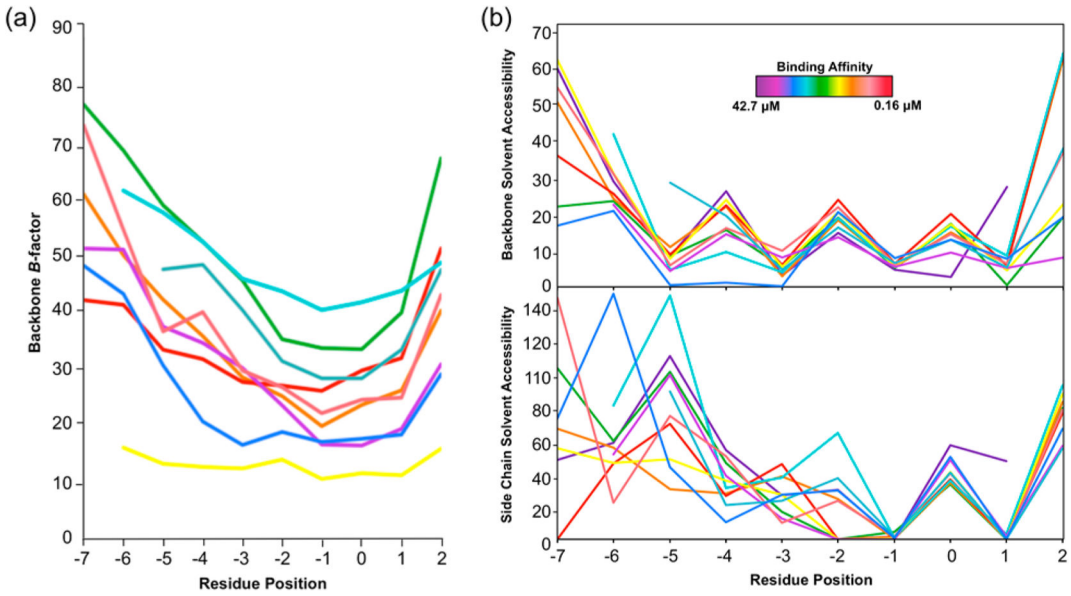

Figure 8.

Peptides bound to LC8 exhibit *B*-factors and solvent accessibility patterns that support the anchored flexibility model. (a) The *B*-factors for backbone atoms of peptides in the LC8 peptide complex are plotted against residue position. *B*-factors for backbone or side chain atoms were averaged using the program "baverage" available through the CCP4 suite.[44] (b) Solvent accessible surface areas per residue for motif residues in the LC8 peptide complex are plotted for each residue position for both backbone atoms (top) and side chains atoms (bottom) in units of $Å^2$. Solvent accessibility was calculated using the Web server GetArea[51] and a van der Waals radius of 1.4 Å. Each plotted motif is colored according to a binding affinity scale where red is the tightest and purple is the weakest. They correspond to Nek9[16] (red), Chica QT1p (pink), Swallow[12] (orange), Ana2 QT1p[14] (yellow), nNOS[13] (green), IC[12] (cyan), Chica QT4p (teal), myosin 5a[17] (blue), Ana2 QT2p[14] (purple), and Pak1[19] (dark purple). Pak1 is not included in panel a.

Author Manuscript Author Manuscript Author Manuscript Author Manuscript

Table 1.

Thermodynamic Parameters of the LC8-Chica Interactions

construct	construct sequence[a]	*N*	K_d (*μ*M)	Δ*H* (kcal/mol)	*T*Δ*S*(kcal/mol)	Δ*G* (kcal/mol)
$Chica_{410–478}$		3	0.4 ± 0.1	−7.6 ± 0.2	1.2 ± 0.4	−8.8 ± 0.2
QT1p (414–424)	SYRKAIDAATQTEE	1	0.4 ± 0.1	−6.8 ± 0.2	1.9 ± 0.2	−8.7 ± 0.2
QT2p (433–443)	SYSVSEVGTQTSI	1	6.3 ± 0.4	−8.5 ± 1.1	−1.4 ± 1.1	−7.1 ± 0.04
QT3p (444–454)	SYTTACAGTQTAV		ND			
QT4p (466–476)	SYWSRSTTTQTDM	1	5.2 ± 0.1	−8.2 ± 0.1	−1.2 ± 0.3	−7.0 ± 0.2

[a]Non-native residues added to the N-terminus of each peptide to increase solubility and improve concentration determination are underlined.

Biochemistry. Author manuscript; available in PMC 2020 February 01.

Author Manuscript Author Manuscript Author Manuscript Author Manuscript

Biochemistry. Author manuscript; available in PMC 2020 February 01.

Table 2.

Data Collection and Refinement Statistics of X-ray Crystal Structures

	PDB code: 5E0L	**PDB-code: 5E0M**
Data statistics		
structure	LC8-QTlp	LC8-QJ4p
space group	$P6_122$	$P6_122$
unit cell *a, b, c* (Å)	44.67, 44.67, 204.17	44.18, 44.18, 204.71
resolution (Å)	51.01–131 (1.33–1.31)[a]	68.34–1.64 (1.67–1.64)
completeness (%)	100.0 (99.1)	100.0 (100.0)
unique reflections	30438 (1438)	15900 (754)
Multiplicity	30.8 (8.0)	33.4 (24.7)
R_{meas} (%)	8.3[b] (47.9)	37.8[c] (931)
$<I/\sigma>$	20.6[d] (0.4)	9.8[e] (0.5)
$CC_{1/2}$	1.0 (0.26)	1.0 (0.17)
Refinement statistics		
resolution range (Å)	38.7–1.31 (1.35–1.31)	38.6–1.65 (1.78–1.65)
R-factor (%)	19.6 (47.2)	20.7 (44.8)
R_{free} (%)	20.2 (48.2)	23.2 (47.3)
protein residues	97	95
water/SO_4 molecules	59/1	60/2
sulfate molecules	1	2
total atoms	1704	1688
rmsd[f] lengths (Å)	0.014	0.007
rmsd angles (deg)	1.3	1.1
Ramachandran plot[g]		
φ, ψ-preferred (%)	97	97
φ, ψ-allowed (%)	3	3
φ, ψ-outliers (%)	0.0	0.0
B-factors		
<main chain> ($Å^2$)	33	34

Author Manuscript Author Manuscript Author Manuscript Author Manuscript

	PDB code: 5E0L	PDB-code: 5E0M
<side chains and waters> ($Å^2$)	46	45

[a] Values in parentheses are for the highest-resolution shell.

[b] R_{meas} in the inner shell (51.02–7.18 Å) is 4.6%.

[c] R_{meas} in the inner shell (68.34–8.98 Å) is 15.8%.

[d] $<I/\sigma>$ in the inner shell is 75.2 and falls to ~2 at 1.55 Å.

[e] $<I/\sigma>$ in the inner shell is 35.4 and falls to ~2 at 2.1 Å.

[f] rmsd = root-mean-square deviation.

[g] Preferred, allowed, and outlier regions as assigned by Molprobity.